

RESEARCH ARTICLE

Teaching an old dog new tricks: A lipid membrane-based electric immunosensor for real-time probing of the spike S₁ protein subunit from SARS-CoV-2

Alina Asandei¹ | Loredana Mereuta² | Irina Schiopu¹ | Yoonkyung Park³ | Tudor Luchian² 

¹ Sciences Department, Interdisciplinary Research Institute, Alexandru I. Cuza University, Iasi, Romania

² Department of Physics, Alexandru I. Cuza University, Iasi, Romania

³ Department of Biomedical Science and Research Center for Proteinaceous Materials (RCPM), Chosun University, Gwangju, Republic of Korea

Correspondence

Yoonkyung Park, Department of Department of Biomedical Science and Research Center for Proteinaceous Materials (RCPM), Chosun University, Gwangju, Republic of Korea, 61452. Email: y_k_park@chosun.ac.kr
 Tudor Luchian, Department of Physics, Alexandru I. Cuza University, Iasi 700506, Romania. Email: luchian@uaic.ro

Alina Asandei and Loredana Mereuta contributed equally to this work

Funding information

Unitatea Executiva pentru Finantarea Invatamantului Superior, a Cercetarii, Dezvoltarii si Inovarii, Grant/Award Number: PN-III-P4-ID-PCE-2020-0011

Abstract

Fast, cheap, and easy to implement point-of-care testing for various pathogens constituted a game changer in past years due to its potential for early disease diagnosis. Herein, we report on the proof-of-concept of a simple method enabling in vitro detection of a structural spike protein subunit from the SARS-CoV-2 (S₁) in aqueous samples. At the core of this discovery lies the well-known paradigm of monitoring the capacitive current across a reconstituted zwitterionic lipid membrane subjected to a periodic transmembrane potential, followed by the real-time spectral analysis enabling the extraction of the second harmonic of the capacitive current. Subsequent changes in the amplitude of this harmonic recorded during lipid membrane–S₁ interactions were correlated with alterations induced in the inner membrane potential profile by the S₁ protein subunit adsorption, and were shown to be augmented by ionic strength, the presence of a specific monoclonal antibody designed against the S₁ subunit and the angiotensin-converting enzyme 2 (ACE2) protein receptor, and uninhibited by the presence of other human serum proteins.

KEYWORDS

ACE2, antibody, lipid membrane, membrane potential, SARS-CoV-2 spike S₁

1 | INTRODUCTION

Coronavirus disease 2019 (COVID-19) is a highly contagious infectious disease caused by the severe acute respiratory syndrome coronavirus 2 (SARS-CoV-2), and since its first report in December 2019, it has spread worldwide reaching 154,815,600 cases by May 6, 2021 [1] and

became a devastating pandemic [2]. Early accurate diagnosis is crucial for controlling the pandemic, and a wide number of assays ranging from molecular, serological, and immunological-based approaches (e.g., reverse transcription–polymerase chain reaction, cutting-edge CRISPR-related methods) to classical diagnostic methods (e.g., chest CT scans) have helped scientists and physicians to screen and diagnose SARS-CoV-2 infection [3].

These testing methods still pose challenges in field practice mainly due to the high cost and intricacies related to sample-preparation, expensive instrumentation facility, and skilled personnel needed. For the convenient, accurate, and rapid diagnosis of SARSCoV-2 infection, the deployment of real-time, rapid testing kits, and point of care tests

Abbreviations: COVID-19, coronavirus disease 2019; SARS-CoV-2, severe acute respiratory syndrome coronavirus 2; ACE2, angiotensin-converting enzyme 2; RBD, receptor-binding domain; S₁, SARS-CoV-2 S₁ subunit; MERS, Middle East Respiratory Syndrome; MERS S₁, MERS-CoV spike S₁ subunit; KCl, potassium chloride; HS, human serum; SDS, sodium dodecyl sulfate; HEPES, hexadecane and 4-(2-hydroxyethyl)-1-piperazineethanesulfonic acid; DPhPC, 1,2-diphytanoyl-sn-glycerophosphocholine; BLM, bilayer lipid membrane; FFT, fast Fourier transform; EMBL-EBI, European Bioinformatics Institute

freed from the need of expensive equipment remains critical. For such tasks and based on the cited examples, the four structural proteins of SARS-CoV-2, namely the spike surface glycoprotein (S), small envelope protein (E), matrix protein (M), and nucleocapsid protein (N), as well as their gene sequences and antibodies, could be used as targets for detection. The coronavirus entry into host cells and subsequent human pathogenicity is mediated by its 150 kDa transmembrane spike (S), heavily N-linked glycosylated homotrimer glycoprotein, comprising two functional subunits responsible for binding to the host cell receptor (S_1 subunit) with the receptor-binding domain (RBD) and fusion of the viral and cellular membranes (S_2 subunit) [4–6]. It is also known that for cell entry, SARS-CoV-2 specifically targets the transmembrane human angiotensin-converting enzyme 2 (ACE2) [7, 8], with an affinity in the low nanomolar range [9]. As a viable alternative to the detection methods noted above, electrochemical biosensing platforms comprising bio-recognition elements (e.g., specific antibodies) and signal transducers enabled the direct detection of various respiratory viruses [10] including SARS-CoV-2 [11].

In a recent effort made from our group toward with the established nanopore system [12, 13], we showed that the S_1 subunit of the SARS-CoV-2 spike protein attaches to and permeabilizes lipid bilayer membranes even in the absence of a specific receptor protein [14]. Inspired from previous work on membrane-active peptides [15, 16], we hypothesized that prior to permeabilization, the lipid membrane adsorption of the S_1 subunit from the SARS-CoV-2 spike protein alters the distribution of mobile ions, surface, and polarization charges on the lipid membrane, all leading to changes in the electrical features the membrane, for example, the surface and/or dipole potentials. Here, by exploiting the dependence of the lipid membrane capacitance upon the potential difference across its hydrophobic core, we demonstrate that such changes are readily seen through monitoring the capacitive current across the lipid membrane substrate. Finally, we assemble our findings and propose a deceivingly simple, yet effective biosensing platform that allows for direct detection and recognition of the S_1 protein, based on its specific interaction with a designed monoclonal antibody and the ACE2 receptor, through the response elicited by such complexes on the membrane potentials of a reconstituted planar lipid membrane.

2 | EXPERIMENTAL METHOD AND REAGENTS

The specific SARS-CoV 2 proteins used herein were SARS-CoV-2 Spike S_1 -His Recombinant Protein (cat. #40591-V08H), SARS-CoV-2 Spike S_1 Antibody Rabbit Mab (cat. #40150-R007), MERS-CoV Spike S_1 protein (cat. #40069-V08H), and recombinant human ACE2 (His Tag) (cat. #10108-H08H), all purchased from Sino Biological Europe GmbH (Germany). Potassium chloride (KCl), human serum (HS) (cat. #H4522), sodium dodecyl sulfate (SDS), ultrapure water, *n*-pentane, hexadecane, and 4-(2-hydroxyethyl)-1-piperazineethanesulfonic acid (HEPES) were bought from Sigma-Aldrich (Germany). The 1,2-diphytanoyl-sn-glycerophosphocholine (DPhPC) lipids were procured from Avanti Polar Lipids (Alabaster, AL, USA).

Significance Statement

- A simple method enabling in-vitro detection of a structural spike protein subunit from the SARS-CoV-2 (S_1) in aqueous samples is highly desirable.
- The amplitude of the second harmonic of the capacitive current through a lipid membrane substrate subjected to a periodic potential difference is correlated with alterations induced in the membrane potential profile by the S_1 protein subunit adsorption.
- Such changes are augmented by ionic strength, the presence of a specific monoclonal antibody designed against the S_1 subunit and the human angiotensin-converting enzyme 2 protein receptor (ACE2), and enable S_1 detection in the nanomolar range.

2.1 | Electrophysiology experiments

The symmetrical membrane system used herein was obtained from DPhPC lipids dissolved in HPLC-grade *n*-pentane (10 mg mL⁻¹) as described before [14, 17]. In short, the lipid bilayer (BLM, bilayer lipid membrane) was formed on a pre-treated with 10% v/v hexadecane in highly purified *n*-pentane aperture of ~120 μ m diameter in a 25 μ m thick Teflon film (Goodfellow, Malvern, MA, USA) clamped between two chambers each of 1 mL volume (filled with the electrolyte containing 0.1 M or 2 M KCl buffered at a pH value of ~6.3 in 10 mM HEPES). The recording cell was housed in a Faraday cage (Warner Instruments, USA) and placed on a vibration-free platform (BenchMate 2210, Warner Instruments, USA). All experiments were performed at a room temperature of ~25°C, and all protein stock solutions were kept at -20°C when not used. The working principle used for the automated real-time monitoring and evaluating of the capacitive current through the lipid bilayer was based on the well-established inner field compensation (IFC) method, as previously described [18]. Briefly, we constructed a virtual instrument to collect the capacitive current via Ag/AgCl electrodes coupled with a Multiclamp 700B computer-controlled amplifier or Axopatch 200B instrument (Molecular Devices, USA). Data acquisition was performed with an NI PCI 6221, 16-bit acquisition board (National Instruments, USA) at a sampling frequency of 10 kHz within the LabVIEW 8.20 environment and within the same virtual instrument, we employed fast Fourier transform (FFT) spectral analysis on the recorded capacitive current (I_C) through a lipid membrane subjected to a sinusoidal time-varying potential difference superimposed on a dc bias u_0 ($\Delta V_{\text{ext}} = u_0 + u_1 \sin(2\pi\Delta t)$), with $v = 420$ Hz and $u_1 = 50$ mV—applied from the A/D D/A acquisition card, and digitally extracted and analyzed the power-spectrum-derived amplitude of the harmonic component at the 840 Hz (denoted herein as I_2). The values reflecting time changes in the I_2 amplitude as reported in the main paper were computed and reported as generated within the LabVIEW virtual instrument used throughout. To monitor

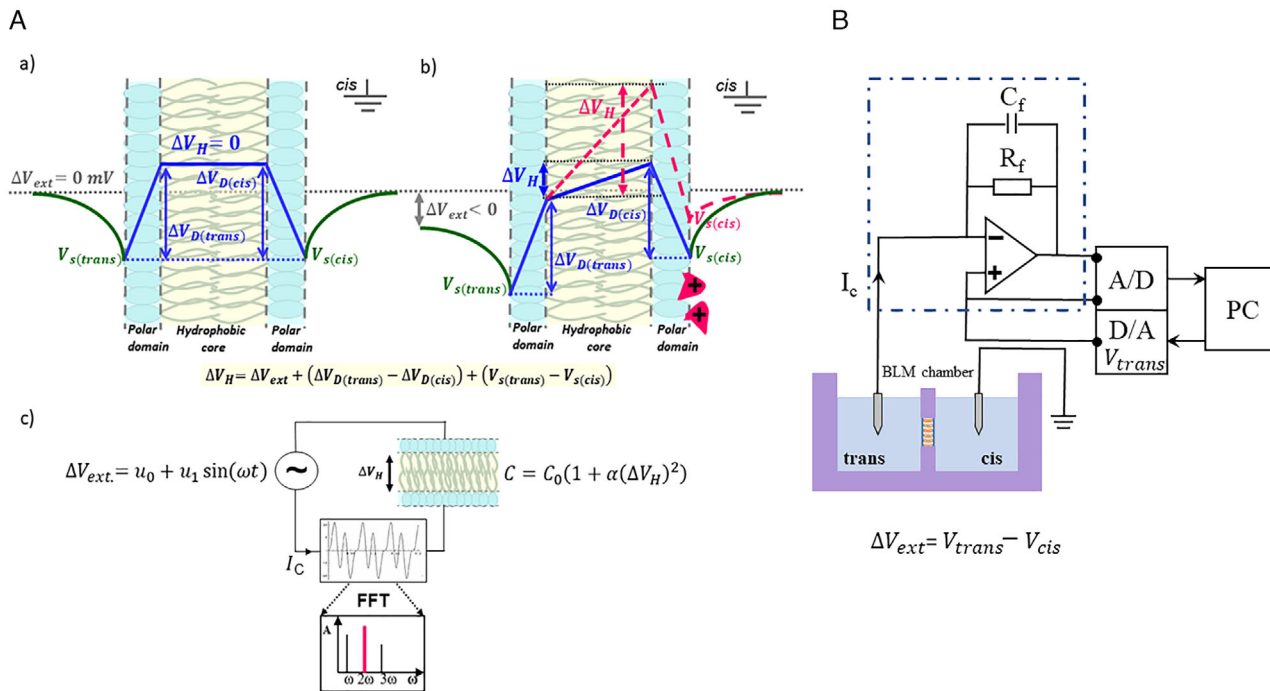


FIGURE 1 (A) Schematic diagram showing the Gouy–Chapman model for the planar lipid membrane surface (V_S) and dipole potential (ΔV_D) profiles [19]. In the symmetrical case, at $\Delta V_{ext} = 0$ (a), the potential difference across the hydrophobic core $\Delta V_H = 0$. (b) For the case of an asymmetrical membrane clamped at $\Delta V_{ext} \neq 0$, the net ΔV_H is also influenced by the asymmetry in the V_S and ΔV_D on the *cis* and *trans* monolayers. (c) Within the elastic capacitor description of the membrane, a periodic ΔV_{ext} results in a time-varying capacitive current (I_C) comprising three harmonics ($\omega, 2\omega, 3\omega$) of the ΔV_{ext} 's pulsation (ω) (see also Figure 2A). (B) Simplified schematics of the experimental setup used herein to apply voltages (ΔV_{ext}) to the lipid membrane and record ensuing capacitive currents (I_C). The dashed-dotted rectangle illustrates the I–V head-stage of the amplifier, fully controlled by the A/D D/A acquisition card via a personal computer (PC)

how the difference in the dipole and surface potential of the membrane unfolds in time as a result of specific interactions with the molecules of interest (i.e., S_1 , ACE2, MERS S_1 , or S_1 – S_1 antibody immunological complex added on the grounded *cis* chamber), the dc bias of the applied voltage signal to the membrane was kept constant ($u_0 = -150$ mV) and the time-evolution of the I_2 was later analyzed. The data handling and graphic representations of the recorded data were done using Origin 6 (OriginLab, Northampton, MA, USA).

3 | RESULTS AND DISCUSSION

3.1 | Physical principle of the detection system

As illustrated in Figure 1A and demonstrated previously [18, 19], in assessing the physical response of a lipid membrane to an applied potential difference (Figure 1B), two considerations are crucial: (i) due to electrostriction effects on an equivalent “elastic” capacitor that models to a first approximation a reconstituted lipid membrane, the membrane capacitance (C) depends quadratically upon the sensed voltage difference (ΔV_H) across its hydrophobic core ($C = C_0(1 + \alpha\Delta V_H^2)$) (C_0 represents for the minimum value of the membrane capacitance at $\Delta V_H = 0$ and $\alpha [V^{-2}]$ is a constant (Supporting Information); (ii) the actual ΔV_H embodies three main contributions, arising from the exter-

nally applied potential difference across the lipid membrane (ΔV_{ext}), the difference on the lipid membrane surface potentials (V_S) measured on both sides of the membrane, and respectively the difference in the membrane dipole potentials (ΔV_D) [20–23], as measured between the *cis* and *trans* monolayers of the membrane.

From elementary electrostatic description and considering the case of an electrically asymmetric membrane, namely surface and dipole potentials assume different values on its *cis* and *trans* sides (i.e., $\Delta V_S = V_{S(trans)} - V_{S(cis)} \neq 0$ and $\Delta\Delta V_D = \Delta V_{D(trans)} - \Delta V_{D(cis)} \neq 0$), it is true that while clamped at a particular external potential difference (ΔV_{ext}), the potential difference across the membrane’s hydrophobic core writes $\Delta V_H = \Delta V_{ext} + \Delta V_S + \Delta\Delta V_D$ (Figure 1Aa,b).

If for a such model lipid membrane, the externally applied potential difference consists of a constant term (u_0) and a sinusoidal component with amplitude (u_1) and pulsation (ω) ($\Delta V_{ext} = u_0 + u_1 \sin(\omega t)$), by virtue of elementary circuit analysis, it follows that the resulting time-dependent capacitive current ($I_C(t)$) embodies three harmonics of the fundamental pulsation (ω) (Supporting Information). For our analysis we focused solely on the second harmonic isolated from the power-spectra of the capacitive current (Figure 2A), which in the time-domain and with the notations employed above writes: $I_2(t) = 3\alpha\omega \sin(2\omega) C_0 (\delta + u_0) u_1^2$. In this expression, the term δ stands for the lumped ($\Delta V_S + \Delta\Delta V_D$) value quantifying the asymmetry in the surface and dipole potential of the lipid membrane (Supporting Informa-

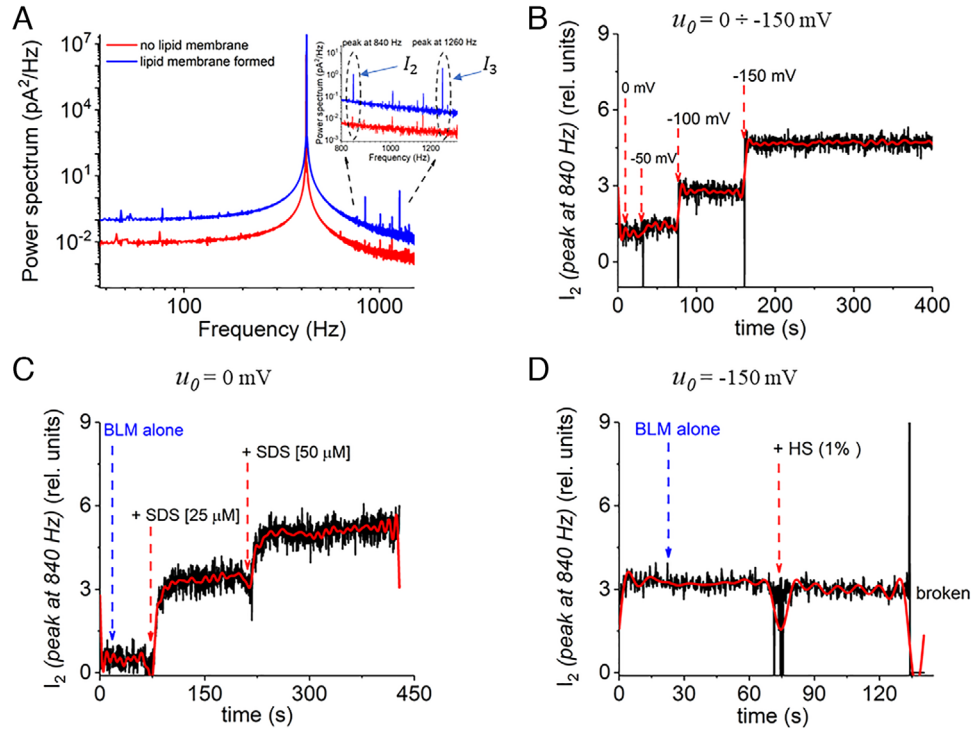


FIGURE 2 (A) Typical representation of the power-spectra data on the capacitive current (I_C) measured in the “open air” (no lipid membrane formed) and respectively after the successful formation of a lipid membrane, subjected to a periodic ΔV_{ext} with zero dc bias (u_0) ($\Delta V_{\text{ext}} = u_1 \sin(2\pi\nu t)$; $\nu = 420 \text{ Hz}$ and $u_1 = 50 \text{ mV}$). In the latter case (“lipid membrane formed”), besides the fundamental harmonic measured at 420 Hz, the spectral analysis reveals the presence of two supplementary harmonics measured at 840 Hz (peak denoted herein by I_2) and 1260 Hz (peak denoted herein by I_3) (see the zoomed-in inset, the dashed encircled areas). The fact that the second harmonic (I_2) is non-zero at zero dc bias ($u_0 = 0$) (Supporting Information, “Theoretical account for the electric response of an elastic lipid membrane bilayer”), reflects among others an existing offset between the Ag/AgCl electrodes potentials, equivalent to applying a distinct from nil potential difference across the membrane. (B) The power-spectrum amplitude changes of the second harmonic (I_2) from the capacitive current (I_C) measured across a lipid membrane subjected to a periodic ΔV_{ext} ($\Delta V_{\text{ext}} = u_0 + u_1 \sin(2\pi\nu t)$; $\nu = 420 \text{ Hz}$ and $u_1 = 50 \text{ mV}$) with variable dc bias (u_0) (at $u_0 = -50, -100$, and -150 mV , the percent increase of I_2 was 25%, 140%, and 308%, respectively), with dc bias $u_0 = 0$ but exposed asymmetrically (*cis* side only) to SDS (C) (440% increase of I_2 after addition SDS [25 μM] and respectively 740% after addition SDS [50 μM]), and at constant dc bias ($u_0 = -150 \text{ mV}$) but exposed asymmetrically (*cis* side only) to human serum (HS 1%) (D). HS, human serum; SDS, sodium dodecyl sulfate

tion). It then follows that if the adsorption of certain membrane active molecules induces changes determines an asymmetry of the surface or dipole potentials (or both), the analyte detection can be easily achieved through monitoring the amplitude second harmonic in the capacitive current across the membrane. Moreover, the time course of this harmonic amplitude would correlate with the adsorption kinetics of the membrane active molecules under study.

To test our system, in a first set of control experiments we maintained the symmetry of a reconstituted lipid membrane and increased in a stepwise manner the value of constant term (u_0) of the ΔV_{ext} . As expected, the FFT spectral analysis of the resulting I_C clearly indicated a corresponding stepwise increase in the power-spectral amplitude of the second harmonic of the capacitive current, called herein I_2 (Figure 2B).

Then, we maintained fixed values on the amplitude components of the ΔV_{ext} but added on one side of the membrane SDS, an anionic amphiphile whose adsorption at the lipid membrane interface induces a negative surface charge density σ [electronic charges/ \AA^2] and alters the surface potential V_5 [mV] of the membrane only of the addition side

of the amphiphile, according to $\sigma = \pm \sqrt{2\epsilon_r\epsilon_0RT \sum_{i=1}^2 C_i (e^{-\frac{z_i F V_5}{RT}} - 1)}$ [20, 24]. In this formula, C_i and z_i refer to the molar concentration and valence of the i th salt species in the bath, R is the general gas constant, F the Faraday’s constant, T the absolute temperature, and ϵ_r and ϵ_0 are the relative permittivity of the electrolyte and vacuum permittivity, respectively. By virtue of principles underlined above, increasing amounts of the SDS led to proportional augmentations in the amplitude of the I_2 (Figure 2C). Unlike the previous case, the time-dependent unfolding of such changes is distinct from a stepwise-like pattern and correlates with the time-dependent, diffusion-controlled SDS adsorption kinetics on the membrane interface. As a supplementary test for the detection selectivity in physiologically relevant samples, one-side addition of 1% HS under fixed ΔV_{ext} left the electric characteristics of the lipid membrane largely unaffected, as judged from non-significant changes in the I_2 (Figure 2D). At this point, we firmly concluded that a simple testing system as employed herein may indeed be capable of accurate real-time monitoring of the presence of a soluble analyte, if its adsorption on the lipid membrane alters its electric properties.

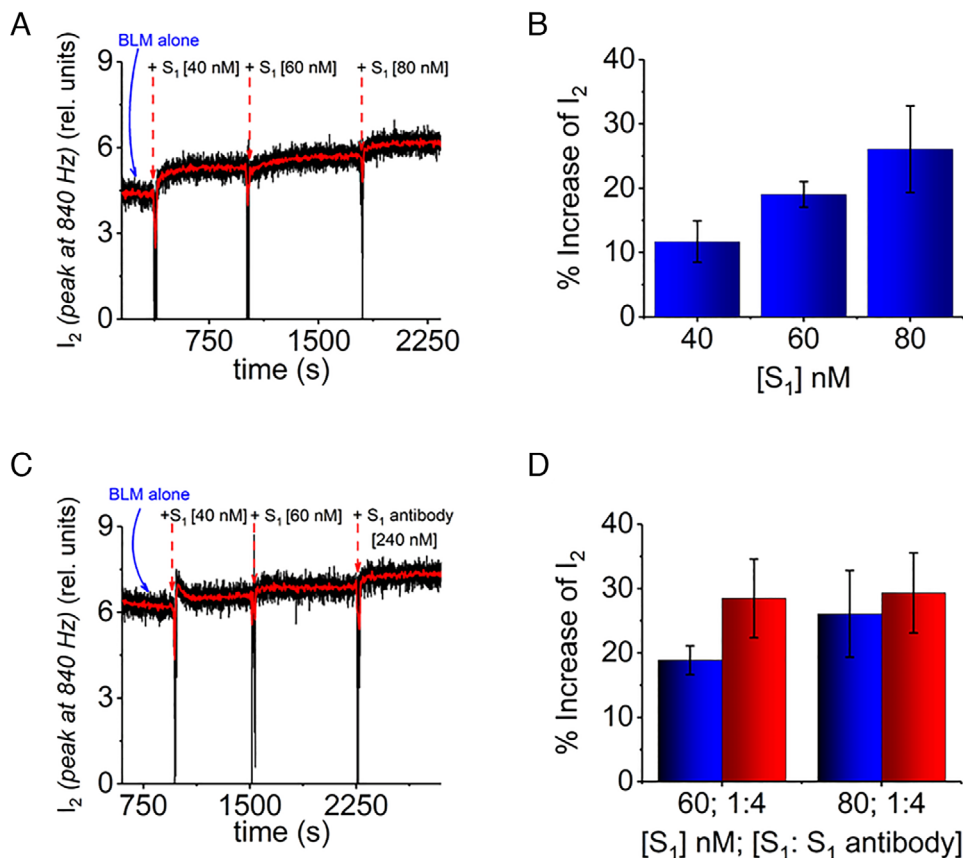


FIGURE 3 (A) When a lipid membrane is subjected to a periodic $\Delta V_{\text{ext}} = u_0 + u_1 \sin(2\pi\nu t)$ ($u_0 = -150 \text{ mV}$, $\nu = 420 \text{ Hz}$ and $u_1 = 50 \text{ mV}$), incremental asymmetrical additions of the S_1 subunit (*cis* side) led to correspondingly increasing amplitudes of the I_2 current harmonic, quantified in (B). (C) In the presence of S_1 antibody, the amplitude of the I_2 current harmonic increased further, as quantified in (D) (red bars; I_2 measured with the S_1 - S_1 antibody complex and blue bars I_2 measured with the S_1 alone)

3.2 | Detection of the S_1 subunit protein in buffer

In Figure 3, we present typical traces reflecting changes in the amplitude of the I_2 across a reconstituted lipid membrane, following asymmetric addition (*cis* side only) of nM amounts of the SARS-CoV-2 S_1 subunit (S_1), which we already established that adsorbs to the membrane [14]. As seen, incremental concentrations of the added S_1 determine a correspondingly increase in the I_2 amplitude. According to the manufacturer's information, the pI value of the S_1 subunit is 8.25, so that around pH 6.3 as used herein it carries a net positive charge. This suggests that increasing amplitudes of I_2 reflect incremental accumulation of a net positive charge on the membrane interface and a consequent *cis* side surface potential ($V_{S(\text{cis})}$) bias toward more positive values. Notably, time-resolved traces shown in Figure 3 reflect in a real-time manner the lipid membrane- S_1 adsorption kinetics. From a simple electrical perspective, at fixed ΔV_{ext} and similar and unaltered membrane dipole potentials (ΔV_D) on both membrane monolayers, positive changes in the V_S manifested solely on the S_1 addition side of the membrane interface, are equivalent with an increase in the net potential difference sensed across the membrane's hydrophobic core (ΔV_H), equivalent with a membrane hyperpolarization (Figure 1Ab, red line). This is in agreement with the control experiments as shown in

Figure 2A, in which larger potential differences across the membrane translate into correspondingly larger I_2 amplitudes.

3.3 | Detection of the S_1 protein subunit in the presence of specific binding substrates and human serum

For probing the detection specificity, our strategy involved the use of specific molecular substrates for the S_1 subunit, namely a synthesized monoclonal antibody and the ACE2 receptor. As shown in Figure 3, following incremental addition of S_1 and assessment of I_2 changes the final injection of a monoclonal antibody (S_1 antibody) as to achieve a 1:4 (S_1 - S_1 antibody) molar ratio, determined a further augmentation in the I_2 amplitude. In a versatility test, a similar effect was seen in other experiments carried out in similar conditions, where the MERS-CoV spike S_1 subunit (MERS S_1) was employed instead (Figure S1). One should note that such effects are solely attributable for the resulting S_1 - S_1 antibody complex generated in the buffer, as by itself the S_1 antibody does not generate any distinguishable change in the I_2 amplitude (Figure S2). To rationalize the lack of effect generated by the S_1 antibody alone, one must recall that according to the manufacturer,

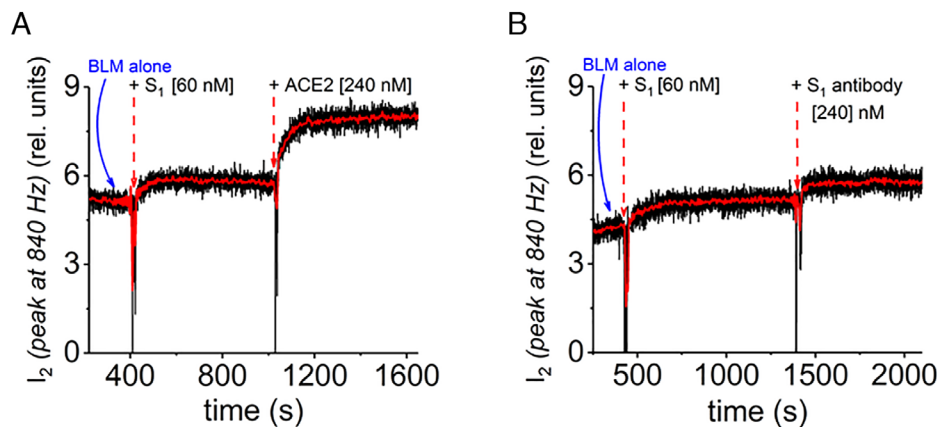


FIGURE 4 In the presence of ACE2, the I_2 amplitude from the capacitive current through the membrane bathed in a buffer containing S_1 [60 nM] and in response to $\Delta V_{\text{ext}} = u_0 + u_1 \sin(2\pi \nu t)$ ($u_0 = -150 \text{ mV}$, $\nu = 420 \text{ Hz}$ and $u_1 = 50 \text{ mV}$), increased by $43.1 \pm 9\%$ (A), whereas a similar concentration of the S_1 antibody led to a smaller increase of $28.5 \pm 6.1\%$ (B). ACE2, angiotensin-converting enzyme 2

the S_1 antibody's pI is 6.47 rendering almost void of net electrical charge around pH 6.3 as used herein, thus being less effectively—as compared to the S_1 subunit—engaged in an electrophoretic-driven association with a negatively biased lipid membrane.

To mimic clinical conditions, we assessed the sensing capacity of the system described herein in the presence of commercial human serum added into the recording chamber. This is a vital step for any possible extension of the presented system to a field-deployable biosensor, since real human serum samples contain up to 10^4 proteins [25], which may target the lipid membrane and affect non-specifically the sensitivity and specificity of detection. As we discovered, S_1 protein detection via S_1 - S_1 antibody complex formation and I_2 monitoring was unaffected by the presence of other blood proteins, judged from the fact that supplementary addition of 1% HS did not interfere with the detection process (Figure S3).

In another set of experiments aimed at testing the detection specificity, addition of the more affine ACE2 receptor at a molar ratio of 1:4 (S_1 -ACE2) resulted in an even better S_1 detection response (Figure 4).

To interpret such increases in the I_2 amplitude through the Gouy-Chapman theory correlating surface potential (V_s) changes with the adsorbed analyte-induced surface charge density (σ) modifications [20], a paradox arises. Knowing that at pH 6.3 as used herein, S_1 antibody is almost devoid of electric charge whereas the ACE2 receptor protein is negatively charged (S_1 antibody's $pI = 6.47$, according to the manufacturer and ACE2 receptor's $pI = 5.8$, calculated with the EMBL-EBI search and sequence analysis tools APIs), S_1 - S_1 antibody and S_1 -ACE2 complexes are expected to bear an almost unchanged (S_1 - S_1 antibody) to a lesser positive charge (S_1 -ACE2) as compared to the free S_1 protein. By comparison to the situation when S_1 was present alone in the electrolyte, it is then expected that S_1 -ACE2 would alter to a lesser extent the membrane surface charge density upon adsorption or leave it largely unchanged (S_1 - S_1 antibody), thus entailing smaller to none changes in the resulting ΔV_H and the recorded I_2 amplitude, respectively (Figure 1Ab). This on the other hand is in stark contrast with the experimental findings presented above (Figures 3 and 4). The apparent paradox is further deepened by another obser-

vation, according to which I_2 amplitude changes recorded following membrane interaction with either the S_1 alone or in complexation with the S_1 antibody are augmented in high salt electrolytes (Figure S4). This is again puzzling, as the mobile ions-induced screening effect of the membrane electrostatics becomes prevalent in salt-concentrated electrolytes. Namely, a high versus Low ionic strength buffer is expected to better shield changes in the surface potential and the ensuing intramembrane electric field caused by membrane adsorption of a similar number of charged analytes. In other words and contrary to our findings, the I_2 amplitude should in fact be augmented in a low salt electrolyte. At the present, we can only speculate with regard to the precise molecular mechanism through which such complexes alter the physical properties of the lipid membranes and in accord to our observations. A plausible explanation would be that S_1 - S_1 antibody and S_1 -ACE2 complexes adsorption to the membrane will also increase the membrane dipole potential of the lipid monolayer where they adsorb to ($\Delta V_{D(\text{cis})}$, Figure 1Ab, red lines). This is not unexpected, as previous data with other membrane insoluble analytes have demonstrated such an effect [20]. Moreover, such an effect would be facilitated in high ionic strength electrolytes—as shown herein, since the enhanced salt screening of the net electric charge on the complexes would in fact determine a more efficient accumulation of the complexes at the membrane surface or intercalation into the lipid matrix.

On the longer run, more experiments with different selections of lipid membrane-forming lipids (e.g., charged lipids, cholesterol) and electrolyte pH may also shed more light into the physical mechanism(s) contributing to the effects seen, through additional possible changes involving membrane fluidity and packing.

4 | CONCLUSION

In this report, we established a simple to operate and effective setup to specifically detect in a time-resolved manner the SARS-CoV-2 S_1 protein subunit in aqueous solution and presence of physiologically relevant molecules. The use of both monoclonal antibodies and the

ACE2 receptor, as specific binding substrates, augmented the S₁ detection. The method opens the perspective of fast and cheap detection of other S₁ proteins containing receptor-binding residues mutations, artificial or natural antibodies in the aqueous sample (e.g., IgG and IgM), testing for efficacy of therapeutics-directed inhibitors (e.g., peptides) to the S proteins of SARS-CoV or related viruses, quantification of the adsorption kinetics of the antigen-antibody (receptor) complexes with a lipid membrane substrate of variable and controllable composition, or enable alternatives for monitoring of the interaction of viral antigens with selected protein targets, relevant for the discovery of decoy therapeutic proteins [26]. Despite its simplicity, we stress that the presented approach may evolve as a promising alternative, complementing established serological techniques [3]. In this context, each step toward the identification of target analytes should be optimized in terms of sensitivity, accuracy, and selectivity, starting from sample preparation from clinical sources, library construction of specific antibody/receptor candidates, and data processing. Prospective solutions to this end may include: (i) structure-based design of highly efficacious antibodies/receptors directed at the targeted analyte; (ii) operating the detection in buffers with specific properties in terms of pH, ionic strength to increase both the propensity of target (antigen)-receptor (antibody) complexation as well as subsequent interaction of the formed complex with the lipid membrane substrate. The extension of the method to a portable biosensing platform could be further facilitated by the use of lipid bilayer-coated nanowires or nanofilms, as core sensing elements to detect the virus-specific structural proteins or for screening suitable antibodies, and the implication of micro/nanoelectronics and integrated microfluidics.

ACKNOWLEDGEMENTS

This work was supported by a National Research Foundation of Korea (NRF) grant funded by the Korean Government (No. 2019R1A2B5B03070330, NRF-2017M3A9E4077206) and Institute for Information & Communications Technology Promotion (IITP) grant funded by the Korea government (MSIT) (No. 2017-0-01714) and grants PN-III-P1-1.1-TE-2019-0037, PN-III-P2-2.1-PED-2019-0016, PN-III-P4-ID-PCE-2020-0011.

CONFLICT OF INTEREST

The authors declare no conflict of interest.

DATA AVAILABILITY STATEMENT

The author has provided the required Data Availability Statement, and if applicable, included functional and accurate links to said data therein

ORCID

Tudor Luchian  <https://orcid.org/0000-0002-9388-7266>

REFERENCES

1. Coronavirus disease (COVID-19) – World Health Organization (n.d.). <https://www.who.int/emergencies/diseases/novel-coronavirus-2019> (Accessed May 12, 2021).
2. Jiang, F., Deng, L., Zhang, L., Cai, Y., Cheung, C. W., & Xia, Z. (2020). Review of the clinical characteristics of coronavirus disease 2019 (COVID-19). *Journal of General Internal Medicine*, *35*, 1545–1549.
3. Carter, L. J., Garner, L. V., Smoot, J. W., Li, Y., Zhou, Q., Saveson, C. J., Sasso, J. M., Gregg, A. C., Soares, D. J., Beskid, T. R., Jervay, S. R., & Liu, C. (2020). Assay techniques and test development for COVID-19 diagnosis. *ACS Central Science*, *6*, 591–605.
4. Tortorici, M. A., & Veesler, D. (2019). Structural insights into coronavirus entry. *Advance in Virus Research*, *105*, 93–116.
5. Wrapp, D., Wang, N., Corbett, K. S., Goldsmith, J. A., Hsieh, C.-L., Abiona, O., Graham, B. S., & McLellan, J. S. (2020). Cryo-EM structure of the 2019-nCoV spike in the prefusion conformation. *Science*, *367*, 1260–1263.
6. Shang, J., Ye, G., Shi, Ke, Wan, Y., Luo, C., Aihara, H., Geng, Q., Auerbach, A., & Li, F. (2020). Structural basis of receptor recognition by SARS-CoV-2. *Nature*, *581*, 221–224.
7. Zhang, H., Penninger, J. M., Li, Y., Zhong, N., & Slutsky, A. S. (2020). Angiotensin-converting enzyme 2 (ACE2) as a SARS-CoV-2 receptor: Molecular mechanisms and potential therapeutic target. *Intensive Care Medicine*, *46*, 586–590.
8. Yan, R., Zhang, Y., Li, Y., Xia, Lu, Guo, Y., & Zhou, Q. (2020). Structural basis for the recognition of SARS-CoV-2 by full-length human ACE2. *Science*, *367*, 1444–1448.
9. Lan, J., Ge, J., Yu, J., Shan, S., Zhou, H., Fan, S., Zhang, Q., Shi, X., Wang, Q., Zhang, L., & Wang, X. (2020). Structure of the SARS-CoV-2 spike receptor-binding domain bound to the ACE2 receptor. *Nature*, *581*, 215–220.
10. Zhao, Z., Huang, C., Huang, Z., Lin, F., He, Q., Tao, D., Jaffrezic-Renault, N., & Guo, Z. (2021). Advancements in electrochemical biosensing for respiratory virus detection: A review. *Trends in Analytical Chemistry*, *139*, 116253.
11. Seo, G., Lee, G., Kim, MiJ, Baek, S. H., Choi, M., Ku, K. B., Lee, C. S., Jun, S., Park, D., Kim, HGI, Kim, S. J., Lee, J. O., Kim, B. T., Park, E. C., & Kim, S.II. (2020). Rapid detection of COVID-19 causative virus (SARS-CoV-2) in human nasopharyngeal swab specimens using field-effect transistor-based biosensor. *ACS Nano*, *14*, 5135–5142.
12. Luchian, T., Park, Y., Asandei, A., Schiopu, I., Mereuta, L., & Apetrei, A. (2019). Nanoscale probing of informational polymers with nanopores. Applications to amyloidogenic fragments, peptides, and DNA-PNA hybrids. *Accounts of Chemical Research*, *52*, 267–276.
13. Ciuca, A., Asandei, A., Schiopu, I., Apetrei, A., Mereuta, L., Seo, C.H., Park, Y., & Luchian, T. (2018). Single-molecule, real-time dissecting of peptide nucleic acid-DNA duplexes with a protein nanopore tweezer. *Analytical Chemistry*, *90*, 7682–7690.
14. Asandei, A., Mereuta, L., Schiopu, I., Park, J., Seo, C. H., Park, Y., & Luchian, T. (2020). Non-receptor-mediated lipid membrane permeabilization by the SARS-CoV-2 spike protein S1 subunit. *ACS Applied Materials & Interfaces*, *12*, 55649–55658.
15. Strömstedt, A. A., Ringstad, L., Schmidtchen, A., & Malmsten, M. (2010). Interaction between amphiphilic peptides and phospholipid membranes. *Current Opinion in Colloid and Interface Science*, *15*, 467–478.
16. Mereuta, L., Luchian, T., Park, Y., & Hahn, K. S. (2008). Single-molecule investigation of the interactions between reconstituted planar lipid membranes and an analogue of the HP(2-20) antimicrobial peptide. *Biochemical and Biophysical Research Communications*, *373*, 467–472.
17. Montal, M., & Mueller, P. (1972). Formation of bimolecular membranes from lipid monolayers and a study of their electrical properties. *Proceedings of the National Academy of Sciences of the United States of America*, *69*, 3561–3566.
18. Mereuta, L., & Luchian, T. (2006). A virtual instrumentation based protocol for the automated implementation of the inner field compensation method. *Central European Journal de Physique*, *4*, 405–416.

19. Haggé, S. O., Wiese, A., Seydel, U., & Gutschmann, T. (2004). Inner field compensation as a tool for the characterization of asymmetric membranes and peptide-membrane interactions. *Biophysical Journal*, *86*, 913–922.
20. Cevc, G. (1990). Membrane electrostatics. *Biochimica et Biophysica Acta*, *1031*, 311–382.
21. Wang, L. (2012). Measurements and implications of the membrane dipole potential. *Annual Review of Biochemistry*, *81*, 615–635.
22. Efimova, S. S., Schagina, L. V., & Ostroumova, O. S. (2014). Channel-forming activity of cecropins in lipid bilayers: Effect of agents modifying the membrane dipole potential. *Langmuir*, *30*, 7884–7892.
23. Duffin, R. L., Garrett, M. P., Thompson, K. B., & Busath, D. D. (2003). Modulation of Lipid bilayer interfacial dipole potential by phloretin, RH421, and 6-ketocholestanol as probed by gramicidin channel conductance. *Langmuir*, *19*, 3561–3563.
24. Mereuta, L., Asandei, A., & Luchian, T. (2011). Meet me on the other side: Trans-bilayer modulation of a model voltage-gated ion channel activity by membrane electrostatics asymmetry. *PLoS One*, *6*, e25276.
25. Anderson, N. L., & Anderson, N. G. (2002). The human plasma proteome. *Molecular & Cellular Proteomics*, *1*, 845–867.
26. Miller, A., Leach, A., Thomas, J., McAndrew, C., Bentley, E., Mattiuzzo, G., John, L., Mirazimi, A., Harris, G., Gamage, N., Carr, S., Ali, H., Van

Montfort, R., & Rabbitts, T. (2021). A super-potent tetramerized ACE2 protein displays enhanced neutralization of SARS-CoV-2 virus infection. *Scientific Reports*, *11*, 10617.

SUPPORTING INFORMATION

Additional supporting information may be found online <https://doi.org/10.1002/pmic.202100047> in the Supporting Information section at the end of the article.

How to cite this article: Asandei, A., Mereuta, L., Schiopu, I., Park, Y., & Luchian, T. (2022). Teaching an old dog new tricks: A lipid membrane-based electric immunosensor for real-time probing of the spike S₁ protein subunit from SARS-CoV-2. *Proteomics*, *22*, e2100047. <https://doi.org/10.1002/pmic.202100047>